Flow processes and pressure evolution in aquifers during the injection of supercritical CO_2 as a greenhouse gas mitigation measure

R.A.Chadwick, D.J.Noy & S. Holloway

British Geological Survey, Kingsley Dunham Centre, Keyworth, Nottingham, United Kingdom, NG 12 5GG.

Corresponding author: R.A. Chadwick e-mail: rach@bgs.ac.uk

ABSTRACT:

Regional saline aquifers offer the greatest potential for very large-scale underground CO_2 storage as a means of mitigating greenhouse gas emissions. Their dynamic storage capacity, in terms of induced increases in formation pressure, will limit the rate at which CO_2 can be injected and may ultimately limit the amount of CO_2 that can be stored. Generic flow models have been generated to examine the effects on pressure evolution of various reservoir parameters (dimensions, permeability, porosity, presence and nature of flow barriers). CO_2 injection involves dominantly hydrogeological (single-phase flow) processes in much of the reservoir and surrounding adjacent strata, with additional two-phase flow effects around the CO_2 plume itself. Large, thick aquifers with no significant flow barriers can accept high injection rates (~10 million tonnes of CO_2 per year) without undue pressure effects. However, flow barriers, such as faults, increase induced pressures considerably; for reservoirs with such features, careful site characterisation and operational planning will be required for large storage projects. The principles established from the generic modelling were then applied to a real aquifer storage operation at Sleipner in the North Sea. Here CO_2 is being injected into the Utsira Sand, a large relatively homogeneous reservoir. Modelling indicates that pressure increase should be negligible. In fact observed wellhead pressures do show a small rise, but this can be attributed to temperature changes in the fluid column in the wellbore. Pressure changes in the reservoir are likely to be very small.

KEYWORDS: Carbon storage, reservoir simulation, aquifer, CO_2, greenhouse gas, global warming, climate change.

INTRODUCTION

Capture of CO_2 from industrial point sources and long-term storage in underground geological formations (Holloway 2001) offers a viable means of contributing to an overall global warming mitigation strategy (IPCC 2007). A number of projects involving the underground storage of CO_2 are currently in progress worldwide. These range from industrial operations injecting around 1Mt of CO_2 per year, to much smaller-scale research projects injecting thousands of tonnes and aimed at learning more about reservoir processes associated with CO_2 injection. Examples of the former include natural gas processing at Sleipner in the North Sea (Baklid *et al.* 1996), at In Salah in Algeria (Riddiford *et al*. 2003) and enhanced oil recovery at Weyburn in Canada (Wilson & Monea 2004). Examples of smaller-scale projects include the Nagakoa pilot project in Japan (Kikuta *et al.* 2005) and the Frio brine project in Texas (Hovorka 2005).

These projects have demonstrated the feasibility of injecting CO_2 into subsurface geological reservoirs and are providing valuable test-beds for ongoing scientific research into issues such as time-lapse geophysical monitoring, reservoir history matching, reaction-transport modelling etc. So far, however, a key requirement of large-scale future underground storage - the ability to inject very large volumes of CO_2 (hundreds of Mt) at high rates (5 to 20 Mt per year), remains relatively untested.

Regional-scale saline aquifers have been identified as offering the greatest ultimate potential for very large-scale CO_2 storage (Benson *et al.* 2005). The simplest estimate of the static storage capacity of an aquifer corresponds directly to the volume of available pore-space. Thus, the Triassic Bunter Sandstone Formation in the UK sector of the Southern North Sea, has an estimated total pore volume of 1.10×10^{11} m^3 within closed structures and could contain some 70000 Mt of CO_2 if all this pore-space could be utilised (Chadwick *et al.* 2004a). A number of processes, however, act to reduce the efficiency with which CO_2 can replace the *in situ* formation water and render simple estimates of available pore-space volumetrics unrealistic. These processes fall into three main categories: two-phase flow effects involving the migration of the CO_2 plume itself (including capillary entry effects, residual saturations, relative permeabilities, viscous fingering etc), geochemical reactivity between the CO_2 and formation waters and minerals, and single-phase flow effects associated with the requirement to displace large volumes of water within and around the storage aquifer. Considerable research has been carried out in the first two areas (e.g. Lindeberg & Wessel-Berg 1997; Lindeberg *et al*. 2001; Ennis-King & Paterson 2001; Johnson & Nitao 2003; Czernichowski-Lauriol et al. 2003), but systematic assessment of regional single-phase flow issues remains somewhat neglected, and it is here that this paper will concentrate.

As CO_2 is injected into the pore spaces of the storage aquifer, it displaces much of the *in situ* pore-water. This process causes a progressive increase in formation fluid pressure, centred on the injection point and exacerbated by high injection rates, low reservoir permeability, and the presence of barriers to fluid flow, such as faults. CO_2 is a buoyant fluid under reservoir conditions and storage reservoirs require an overlying capillary seal to retain CO_2 securely. If fluid pressure increases above certain thresholds, faulting or fracturing of the caprock will be induced, and damage

to well-bores in the reservoir may also occur. Both may have serious implications for storage security. Thus, in a storage operation, a geomechanically determined pressure threshold can be established, above which pressure should not rise (Law 1996; Obdam *et al.* 2003). Consequently, pressure increase will limit the rate at which CO_2 can be injected, and ultimately may limit the amount of CO_2 that can be practically stored. The capacity of a reservoir to accept injected CO_2 at a specified rate, and for the required cumulative amount, is termed reservoir injectivity.

This paper uses simplified numerical flow models of generic reservoirs to investigate how stratigraphical and structural properties of the reservoir and seal formations can affect injectivity. The generic methodology is then applied to, and tested on, a real case-study at Sleipner.

Model setup

A basic criterion for the underground storage of CO_2 is that it be at depths greater than around 800 m, at pressures (>8 MPa) where the CO_2 is in a relatively dense fluid phase, typically 500 to 700 kgm^{-3} (e.g. Span & Wagner 1996). This permits much greater storage efficiency, in terms of stored mass per unit reservoir volume, than for gaseous CO_2 at shallower depths. Current CO_2 storage operations are in the depth range 800 to around 2000 m, in reservoirs typically ranging from a few tens of metres to ~ 250 m thick.

In line with this current practice, our baseline generic aquifer model includes a 100 m thick homogeneous sand reservoir, of porosity 30%, with a top surface at 1500 m depth. This is overlain by a 10 m thick overburden layer (the caprock) and is underlain by a similar underburden layer, both of very low permeability and high capillary entry pressure (Fig. 1). The modelling neglects any potential chemical reactivity of CO_2. In fact experimental modelling studies (summarised in Chadwick *et al*. 2008), indicate that geochemical effects of CO_2 on typical argillaceous caprock lithologies will likely be very small.

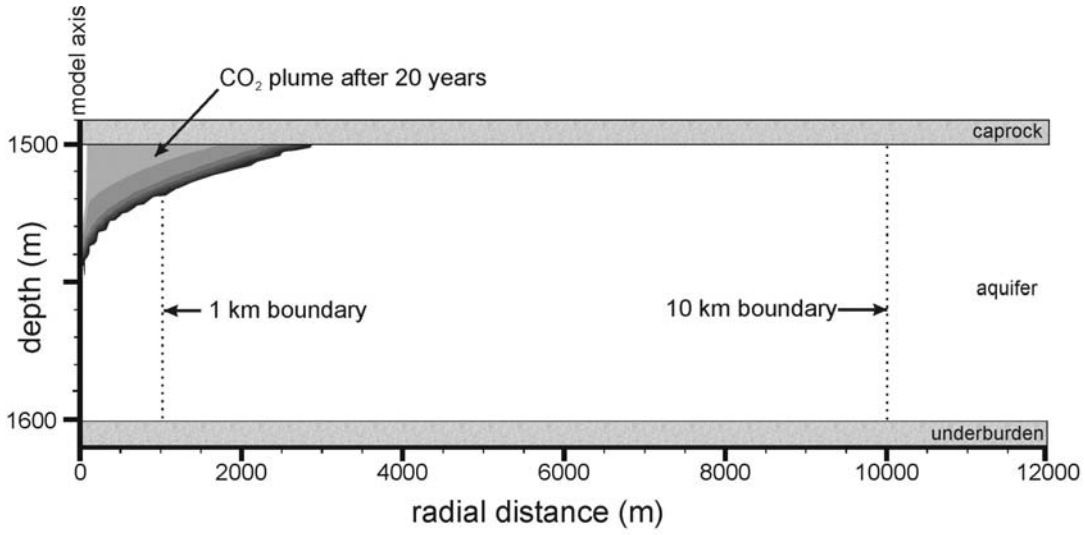

Figure 1 Schematic diagram showing the main elements of the models used in this study. The full models extend to a radial distance of 100 km, plus an additional very large outer grid element. The flow barriers marked are used only in selected models and a further barrier location is included at 35 km. The CO_2 plume shown is an example from the base model calculation. Note strong vertical exaggeration.

We have concentrated in this preliminary study on high permeability aquifers, typified by the Utsira Sand reservoir at Sleipner or by the regional Bunter Sandstone aquifer in the UK. The main physical parameters of the modelling are listed in Table 1.

Table 1. *The main physical parameters of the models considered, with base case values and the ranges examined.*

Parameter	**Base value**	**Range**
Aquifer thickness	100 m	50 – 200 m
Aquifer radius	100+ km	
Aquifer permeability	1 Darcy	0.5 – 10 Darcy
Aquifer porosity	30%	15 – 30%
Injection rate	1 Mt yr^{-1}	1 – 20 Mt yr^{-1}
Pressure at aquifer top	15 MPa	
Temperature at aquifer top	55 ºC	
Geothermal gradient	30 ºC km^{-1}	
Caprock thickness	50 m	
Caprock permeability	0.1 nDarcy	0.1 - 1000 nDarcy
Aquifer P_0	4 kPa	
Caprock P_0	10 MPa	

The model is axisymmetric (radial symmetry), with the injection point on the axis, and a radial element mesh was set up to allow the inclusion of vertical flow barriers

creating cylindrical compartments of various sizes. The radial mesh extends out to 100 km with additional 'very large' (10^{25} m radius) outer elements to set the boundary conditions as approximating to an infinitely large reservoir. Initial P/T conditions were set (Table 1) with hydrostatic fluid pressures. Very large volume elements also provided the boundary conditions for the top and bottom surfaces, effectively fixing the initial values for pressure, temperature, salt mass fraction, and gas saturation at these locations. A salt mass fraction of 0.032 was used throughout, reasonable for a saline storage aquifer. A single injection point was located 10 m below the top of the reservoir at a depth of 1510 m (~15.1 MPa pressure). The mesh element at the injection point is 2 m high and 5 m in radius, giving an injection point cell volume of 157 m^3. Solubility of CO_2 in saline water is also taken into account (Pruess 2005).

The numerical models were calculated using the TOUGH2 reservoir flow simulator (version 2.0) (Pruess *et al*., 1999) incorporating the ECO2N equation-of-state (Pruess 2005). TOUGH2 is a numerical simulator for non-isothermal flows of multicomponent, multiphase fluids in one, two, and three dimensional porous and fractured media. Fluid properties for a variety of systems can be defined through the use of different fluid property modules that can be included during compilation. The ECO2N module includes a comprehensive description of the thermodynamics and thermophysical properties of H_2O - NaCl - CO_2 mixtures. It is designed to reproduce fluid properties to within experimental error for temperatures in the range 10 to 110 ºC, for pressures up to 60 MPa, and for salinities up to full halite saturation.
Relative permeability was modelled with the van Genuchten (1980) equations:

$$k_{rl} = \sqrt{S^*}\left\{1-\left(1-\left[S^*\right]^{1/\lambda}\right)^{\lambda}\right\}^2 \quad (1)$$

where k_{rl} is the aqueous phase relative permeability and S* is the effective saturation given by:

$$S^* = \frac{\left(S_l - S_{lr}\right)}{\left(1 - S_{lr} - S_{gr}\right)} \quad (2)$$

where S_l is the aqueous phase saturation, and S_{lr} and S_{gr} are aqueous and gas phase residual saturations respectively. Throughout this study, λ has been set to 0.4, S_{lr} to 0.2 and S_{gr} to 0.05, following Pruess *et al.* (2002). For the free CO_2 phase, relative permeability is given by the Corey (1954) function:

$$k_{rg} = \left(1 - S^*\right)^2\left(1 - S^{*2}\right) \quad (3)$$

The capillary pressure between the two phases is given by:

$$P_{cap} = -P_0\left(\left[S^*\right]^{-1/\lambda} - 1\right)^{1-\lambda} \quad (4)$$

where P_0 was set to 4 kPa for the reservoir and λ was set to 0.4 as above.

BASIC RESERVOIR SIMULATIONS

The baseline reservoir model was run with the reservoir permeability set to 1 Darcy (10^{-12} m^2) and an injection rate (Q) of 1 $Mt.yr^{-1}$ for 25 years. Reservoir pressure development was computed at five locations, ranging from 2.5 m to 88 km from the injection point (Fig. 2a). It can be seen that pressures in the near-field rise almost instantly to high values very early in the injection history before decaying to a more stable situation in the medium term (~1 to 25 years). Farther from the injection point the initial transient is absent, with pressures showing a small gradual rise with time.

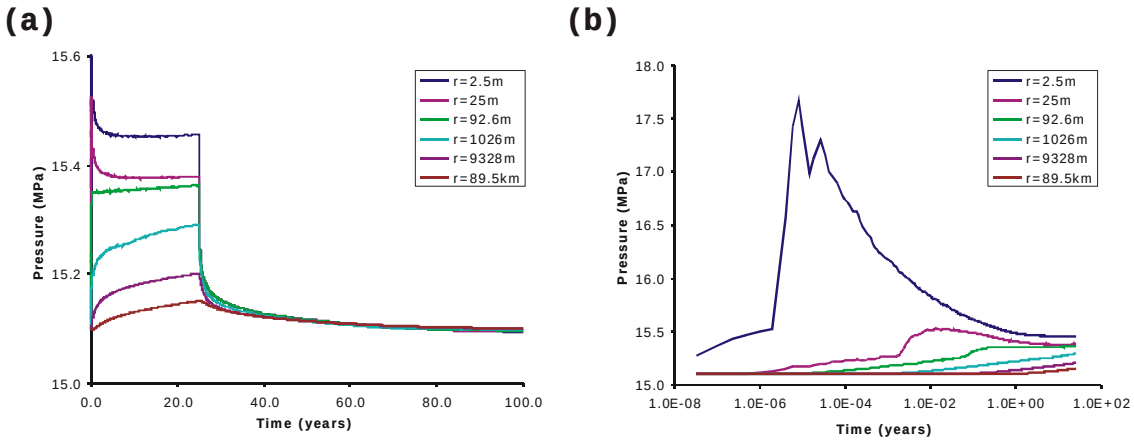

Figure 2 (a) Baseline reservoir model with 25 years of injection at 1 $Mt.yr^{-1}$, including a recovery period of 75 years following the 25 year injection phase, showing pressure evolution at selected points (at distance r from the injection point). (b) Detail of early time pressure responses using logarithmic timescale.

Detail on the initial pressure transient is revealed by using a logarithmic timescale (Fig. 2b). Very high simulated pressures are developed in the near-field during the first hours of injection. This is due to the fact that the full injection rate of 1 $Mt.yr^{-1}$ was imposed instantaneously from t = 0, requiring large amounts of water to be displaced, around a small expanding bubble of CO_2, at high fluid displacement velocities. The transient can be smoothed off as much as required by suitably shaping the injection rate build-up. In fact an initial step up to the full injection rate is unrealistic in terms of actual operational practice where the injection rate would likely be increased gradually over a period of time to control this initial pressure rise. A simulation where the injection rate was progressively increased to 1 $Mt.yr^{-1}$ over a period of one day reduced the peak transient near-field pressure from 17.7 MPa to 16.1 MPa.

Setting aside the initial transient effects, pressure increases in the reservoir range from 0.36 MPa (2.4%) close to the injection point, to less than 0.1 MPa (0.7%) at distances more than about 9 km, with a more-or-less steady-state (inflow = outflow) established in the near-field after a year or so.

Injection rate and permeability effects

The baseline reservoir simulation described above was repeated using injection rates ranging from 1 Mt.yr^{-1} to 20 Mt.yr^{-1}, and with reservoir permeabilities ranging from 0.5 Darcy to 10 Darcy. Pressure in the near-field (r = 2.5m) was calculated at the end of 25 years of injection as a function of injection rate for each value of reservoir permeability (Fig. 3a). It can be seen that, for a given permeability, pressures are approximately linearly proportional to the injection rate. The same data re-plotted to give pressures as a function of permeability for each of the injection rates (Fig. 3b), shows that pressures vary as the near inverse of the permeability, but, in detail, deviate slightly from that functional form. The deviations of these plots from simple reciprocal curves reflect the fact that the density and viscosity of the CO_2 are not constant, but vary over time with pressure and temperature (as determined by the ECO2N equation-of-state module).

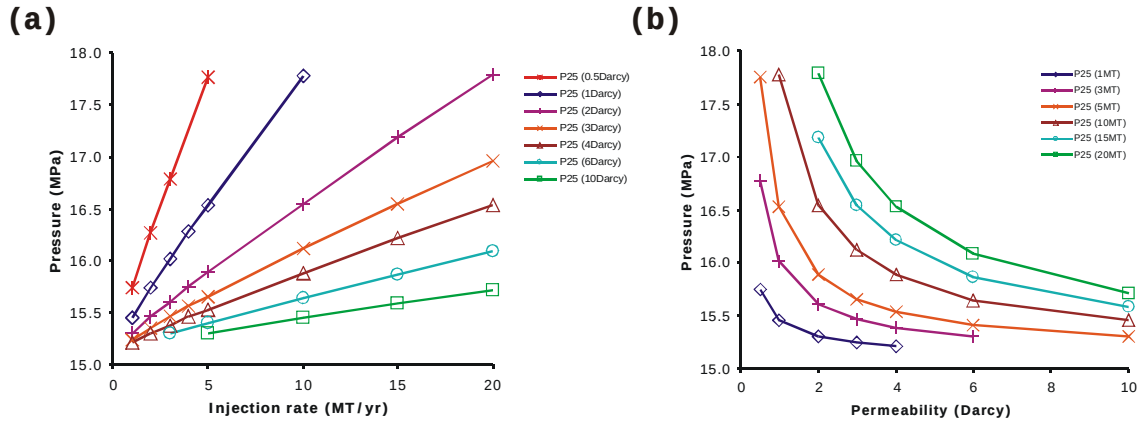

Figure 3 Near-field pressure in the baseline model after 25 years. (a) As a function of injection rate for a range of reservoir permeabilities. (b) As a function of reservoir permeability for a range of injection rates.

Calculated pressures can be contoured over the parameter space defined by reservoir permeability and the injection rate (Fig. 4). Sets of simulations with a range of injection rates and permeabilities were run for high permeability aquifers (Fig. 4a) and for low to medium permeability aquifers (Fig. 4b). Iso-pressure contours pass through the origin and are nearly linear, with a given pressure increase corresponding to a roughly constant ratio of injection rate to permeability (Q/k). This ratio therefore forms a key criterion in determining allowable pressure rise.

So, to illustrate, with baseline reservoir parameters, for the near-field pressure increase to be less than say 10% (15.1 MPa rising to 16.6 MPa), the Q/k ratio must be lower than 5 Mt.yr^{-1}D^{-1}. For high permeability aquifers (Fig. 4a) this criterion generally allows realistic amounts of CO_2 to be injected: 5 Mt.yr^{-1} for a 1 Darcy aquifer, 10 Mt.yr^{-1} for a 2 Darcy aquifer and so on. For medium to low permeability aquifers (Fig. 4b) the situation is not so favourable. A baseline reservoir, of permeability 100 mD, would be able to accept only 0.5 Mt.yr^{-1} without exceeding the nominal 10% pressure increase.

It is important to emphasise however that the simulations are very simple and assume injection from a single well which is intrinsically conservative. In practice, higher injection rates (> 1Mt.yr^{-1} or so) are likely to be accomplished via multiple wells and/or extended perforation intervals which would reduce near-wellbore pressure increase. In addition, pressure increase farther from the injection point (say a few km), is typically just 50 - 60% of the near-field pressure rise (Fig. 2a) and would provide a more reasonable measure of the reservoir performance as a whole.

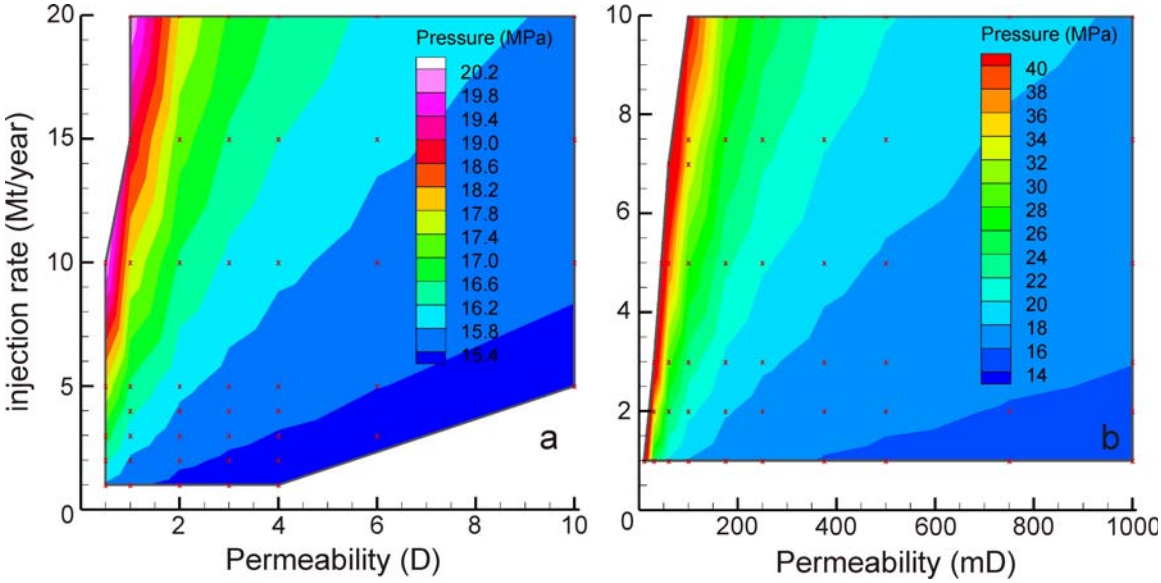

Figure 4 Contoured near-field pressure in the baseline model after 25 years as a function of formation permeability and injection rate. a) High permeability aquifers (b) Low permeability aquifers.

Reservoir 'transmissivity'

In hydrogeology (e.g. Price 1996) the transmissivity of an aquifer is defined as the product of the aquifer thickness and its hydraulic conductivity (a hydrogeological term related to the permeability of an aquifer to water), and is a useful parameter when assessing water resources potential.

To test whether the concept of transmissivity is useful in the context of CO_2 storage, two new models were created; one in which the reservoir was 50 m thick and the other 200 m thick. The models were run with a range of reservoir permeabilities and injection rates, and results grouped into sets for which the product of permeability and reservoir thickness ('transmissivity') is constant (Fig. 5). Results indicate that not only do reservoirs with the same 'transmissivity' give different pressure responses, but the relative order in which the reservoirs plot also varies with 'transmissivity'. This is emphasised where pressure response for each reservoir thickness is plotted against 'transmissivity' for an injection rate of 10 Mt.yr^{-1} (Fig. 6).

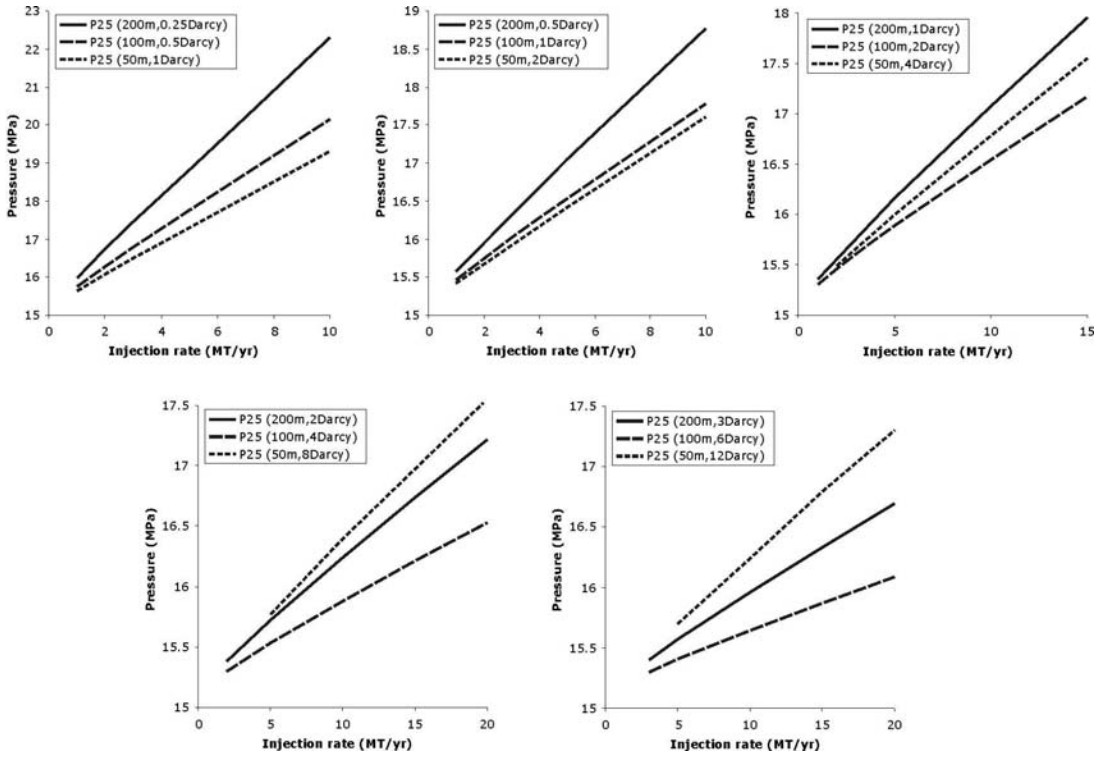

Figure 5 Plots of near-field pressure after 25 years against injection rate for groups of models in which the product of permeability and formation thickness is constant.

At low transmissivities the thick lowest permeability reservoir shows the greatest pressure rise, whereas at high transmissivities the thin, highest permeability reservoir shows the greatest pressure rise. This changing behaviour arises from a number of interacting effects. Firstly, the buoyancy of the CO_2 will generally prevent the plume from accessing the full thickness of the aquifer, so a thin, high permeability aquifer is relatively more efficient at displacing water than a thicker aquifer of equivalent transmissitivity. This is counterbalanced by 'boundary' effects in a thin aquifer that will tend to increase near-field pressures at the expense of pressures farther away. Finally, at low overall transmissivities, thick, low permeability aquifers are relatively inefficient due to the fact that pressure increase becomes increasingly sensitive to permeability decrease (Fig. 3b).

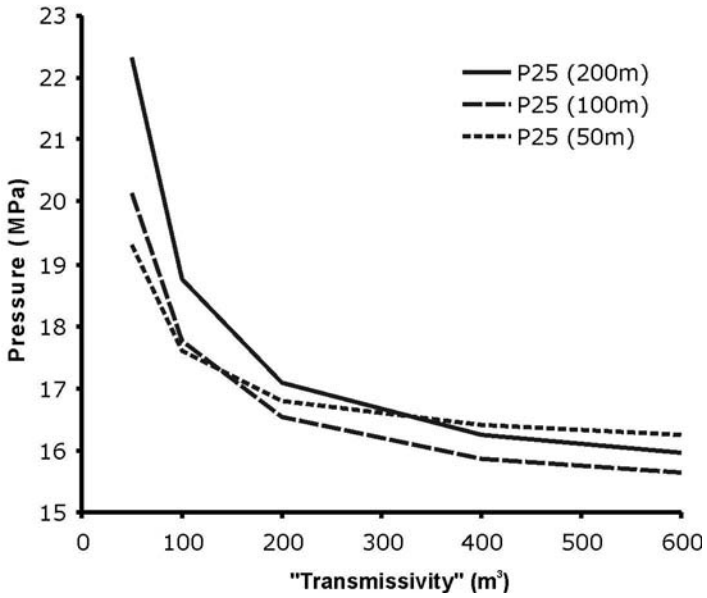

Figure 6 Near-field pressures after 25 years of injection at 10 $Mt.y^{-1}$ into formations of the same 'transmissivity' but different thickness.

Due to these complicating factors, the overall 'transmissivity' of a reservoir seems not to be a particularly useful concept for this type of assessment; the commonly adopted oil industry practice of using explicit values for permeability and formation thickness being supported.

Other minor effects

Further variations of the baseline reservoir model were run with a range of injection rates and permeabilities and with porosity reduced from 30% to 15%. Near-field pressures 25 years after the start of injection can be compared for the two porosities (Table 2). Results indicate that, in an infinite aquifer, for a given permeability, sensitivity to porosity is very small. This is somewhat counterintuitive, but can be explained as follows. For spreading from a single point, the radius of the spreading plume will vary roughly as the cube root of the plume volume and, therefore, as the reciprocal of the reservoir porosity. Fluid displacement velocities will vary similarly. In consequence pressure development will only be weakly dependent on porosity. The main effect of porosity is to change the timescale of the early pressure transient (Fig. 7), the higher porosity reservoir showing a broader transient peak, the timescale of the curves scaling in direct proportion to the porosity.

Table 2. *Near-field pressures after 25 years of injection for a selection of injection rates and formation permeabilities, at two values of formation porosity.*

Q (Mt/yr)	**k** (Darcy)	$\mathbf{P_{25}}(\phi=30\%)$ (MPa)	$\mathbf{P_{25}}(\phi = 15\%)$ (MPa)
1	0.5	15.7424	15.7423
	1	15.4558	15.4600
	2	15.3024	15.3007
	3	15.2445	15.2447
	4	15.2124	15.2122
5	1	16.5349	16.5485
	3	15.6577	15.6441
	6	15.4054	15.4054
10	1	17.7737	17.7898
	3	16.1152	16.0864
	6	15.6444	15.6231
20	1	20.1521	20.1776
	3	16.9582	16.9006
	6	16.0868	16.0414

Although porosity as a discrete parameter is not a key determinant of reservoir pressure in an infinite aquifer, this would not be the case for injection into the finite volumes of a compartmentalised aquifer, where porosity would determine available storage volume. In addition, in real reservoir rocks, porosity and permeability are not usually independent, with lower porosities generally being associated with reduced permeability (e.g. Chilingar *et al.* 1963).

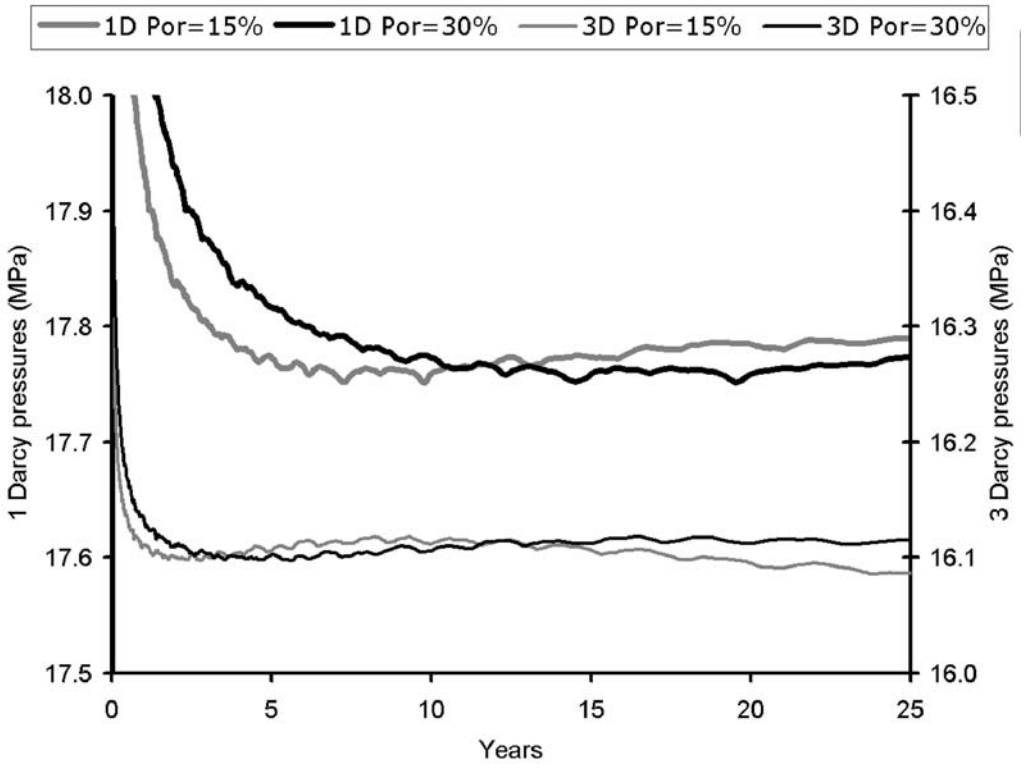

Figure 7 Near-field pressure evolution for the baseline model with a range of porosity and permeability, injecting CO_2 at a rate of 10 $Mt.y^{-1}$.

A second factor that has a potential impact on injection pressures is the permeability of the bounding stratigraphical sealing units, the caprock and underburden. Although these formations are modelled as capillary seals, with high capillary entry pressure to free CO_2 (Table 1), expulsion of water through them (via single-phase flow) will help to reduce reservoir pressure buildup. The baseline model had extremely low caprock and underburden permeabilities of 10^{-22} m^2 (10^{-7} mD). To test the effect of stratigraphical sealing efficacy, additional simulations were run with the permeability of these layers raised to 10^{-19} m^2, a value typical of likely caprock formations for relatively shallow storage reservoirs**.** The results (Table 3) show that such a permeability increase, of three orders of magnitude, reduces the near-field pressures by only a relatively small amount. However a further permeability increase to 10^{-18} m^2 does produce a significantly lower pressure buildup (Fig. 8). It may be noted that in these simplified models the caprock and underburden layers are only 10 m thick. Much thicker sealing units may be likely in reality and these would make proportionately even better bounding seals. Conversely, if the reservoir underburden were not an effective seal, then the effective reservoir thickness could be increased radically and pressures would be reduced accordingly. This effect is not straightforward though, as shown in the section on "transmissivities" – increasing thickness from 100 m to 200 m for a given permeability and injection rate can give a relatively small reduction in pressure.

Table 3. *Near-field pressures after 25 years of injection for a selection of injection rates and formation permeabilities, with two caprock and underburden permeabilities.*

Q (MT/yr)	**k** (Darcy)	$\mathbf{P_{25}}$ ($k_{seal}=10^{-22}$) (MPa)	$\mathbf{P_{25}}$ ($k_{seal}=10^{-19}$) (MPa)
1	1	15.4558	15.4355
	3	15.2445	15.2380
	4	15.2124	15.2099
5	1	16.5349	16.4380
	3	15.6577	15.6255
	6	15.4054	15.3945
10	1	17.7737	17.5874
	3	16.1152	16.0523
	6	15.6444	15.6228
20	1	20.1521	19.7918
	3	16.9582	16.8356
	6	16.0868	16.0489

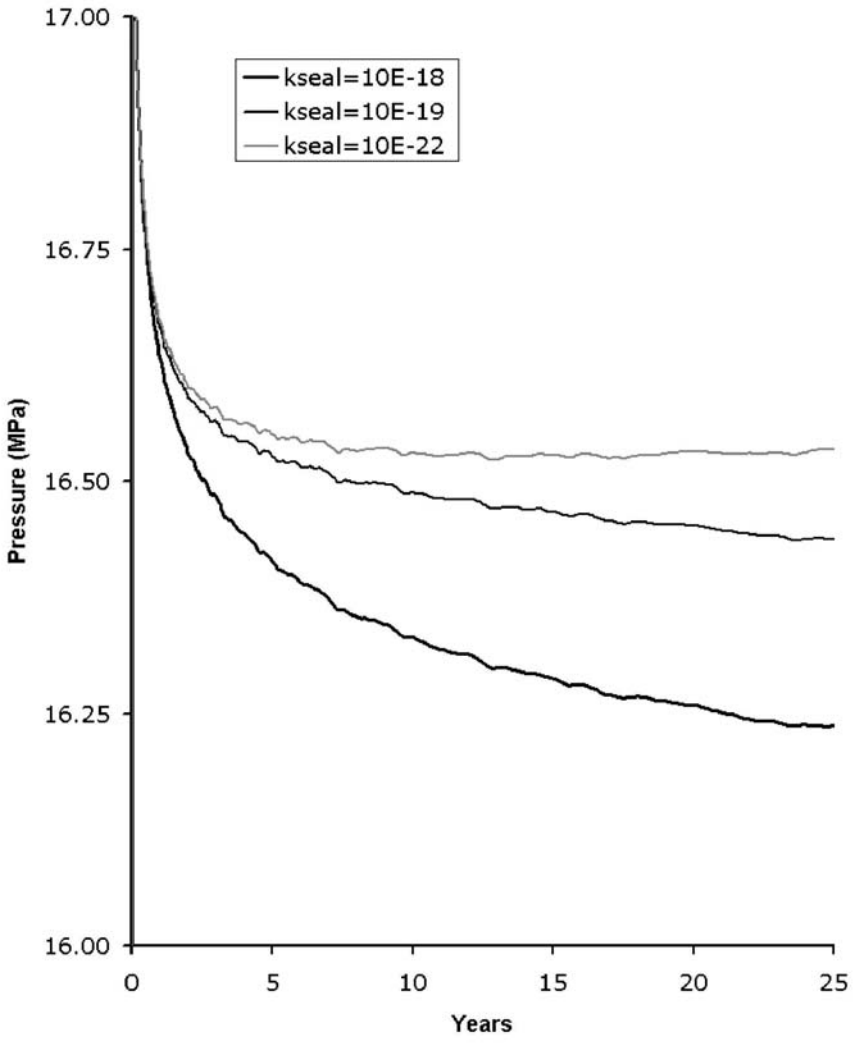

Figure 8 Near-field pressure histories for the baseline reservoir model at an injection rate of 5 Mt.yr^{-1} with a range of sealing layer permeabilities.

RESERVOIR WITH FLOW BARRIERS

It is commonly the case that fluid flow and fluid pressure in hydrocarbon-bearing reservoirs and in aquifers is compartmentalised by low permeability vertical or sub-vertical barriers. These normally correspond to faults and fractures or related features. The flow of multi-phase fluids through flow barriers is a subject of considerable current research in the oil industry (e.g. Berg & Øian 2007). In the context of this paper however, we are principally interested in single-phase flow through faults to assess how easily formation water can be displaced laterally through a reservoir as CO_2 is introduced.

To investigate the effect that flow compartmentalisation has on pressure evolution during and subsequent to CO_2 injection, low permeability vertical elements were introduced into the mesh at various radial distances from the injection point, to produce cylindrical ‘flow barrier’ compartments. Realistic modelling of structurally

highly complex fault zones remains extremely challenging (e.g. Walsh *et al.* 1998), and therefore a very simple representation of the flow barriers is adopted here. Their flow properties have been deliberately set to be conservative (i.e. with effective permeabilities at the low end of the likely natural spectrum) in order to emphasise their potential effect (see Discussion).

Flow barrier at 35 km

The initial simulation took a baseline model, but incorporating a barrier 1 m thick, of permeability 10^{-17} m^2, at a distance of 35 km from the injection point, giving a compartmental area of almost 3850 km^2. CO_2 was injected at a constant rate of 1 $Mt.yr^{-1}$ for 25 years, after which the system was allowed to equilibrate over time, pressure evolution being calculated at a number of locations ranging away from the injection point (Fig. 9a).

Neglecting the initial pressure transient, it is evident that pressures rose significantly above the pre-injection value (15.1 MPa) within the finite injection compartment. After 25 years a pressure increase of 0.43 MPa (~2.8%) had occurred in the near-field, with an increase of 0.18 MPa (~1.2%) at 9 km distance. Pressures were still rising at 25 years, but at a progressively declining rate as the system approached a steady-state. At cessation of injection, removal of the fluid displacement drive allowed pressures everywhere within the compartment to fall almost instantaneously to a nearly uniform value, similar to the pre-cessation value at ~9 km distance. This was followed by a long decay that was almost complete after 100 years. Pressures outside the flow barrier varied only slightly, again peaking at the end of the injection period.

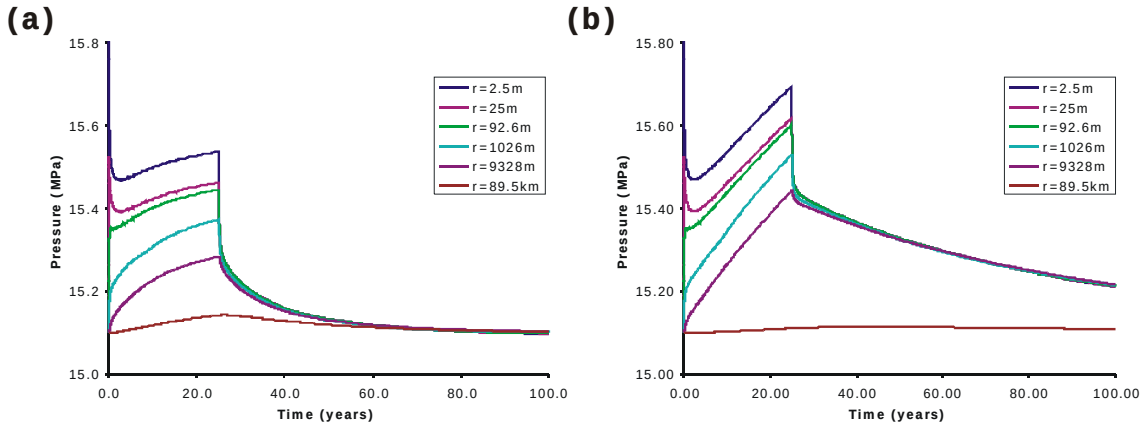

Figure 9 Pressures at selected points in a model with a cylindrical barrier 35 km from the injection point. (a) 1m thick barrier with a permeability of 10^{-17} m^2. (b) 1 m thick barrier with a permeability of 10^{-18} m^2.

The sensitivity of the system to barrier permeability was assessed by re-running the simulation with the barrier permeability reduced by an order of magnitude to 10^{-18} m^2 (Fig. 9b). Within the injection compartment pressures rose much more rapidly during the injection phase with no indication of approaching a steady-state within the 25 year

injection period (see below). After cessation of injection the pressure decline was much slower than for the higher permeability barrier, leaving a residual excess pressure of more than 0.1 MPa after 100 years. Pressures outside the flow barrier showed only very slight perturbation.

Flow barrier at 10 km

The next simulations set the barrier at a distance of 10 km from the injection point, reducing the area of the injection compartment to only 314 km^2. Injection of CO_2 was again stopped after 25 years and the system allowed to equilibrate over time. The flow barrier was assigned permeabilities of 10^{-17} and 10^{-18} m^2 and pressure evolutions calculated (Fig. 10).

In each case the pressures reached were much greater than for the larger compartment, reflecting the smaller pore-volume available to be filled inside the flow barrier. In the case of the higher permeability barrier (Fig. 10a) pressure increase varied from ~0.72 MPa (4.8%) in the near-field to ~0.45 MPa (3%) at ~9 km, with pressures after 25 years close to a steady-state. For the lower permeability barrier (Fig. 10b) pressure rise was distributed more evenly through the compartment, increasing by ~2.7 MPa (17.9%) in the near-field and ~2.4 MPa (15.8%) at ~9 km. Pressures were continuing to rise strongly at 25 years, immediately prior to cessation of injection. Steady-state conditions are reached when the pressure difference across the barrier is sufficient to drive a volumetric flow through it that is equal to the volume of CO_2 being injected. For the higher permeability barrier the pressure difference required is one tenth of that required for the lower permeability barrier, which is why the steady-state is only seen in the former case. As before, a residual excess pressure of around 0.1 MPa remains at 100 years for the 10^{-18} m^2 barrier, but not for the 10^{-17} m^2 one. In both cases pressure changes outside the flow barrier were very small, increasing gently with time as the elevated pressures within the barrier gradually dissipated.

It is clear from the simulations that the total amount of CO_2 that can readily be stored is potentially very sensitive to barrier permeability. The simulations assume a total of 25 Mt of CO_2 storage (1 $Mt.yr^{-1}$ for 25 years). For the higher permeability barrier (Fig. 10a), continued injection for another 40 years or so, giving 65 Mt of storage, would not induce a significant additional increase in formation pressure. In contrast, for the lower permeability barrier (Fig. 10b), continued injection for 40 years would drive peak pressures towards 20 MPa, with consequent potential geomechanical issues.

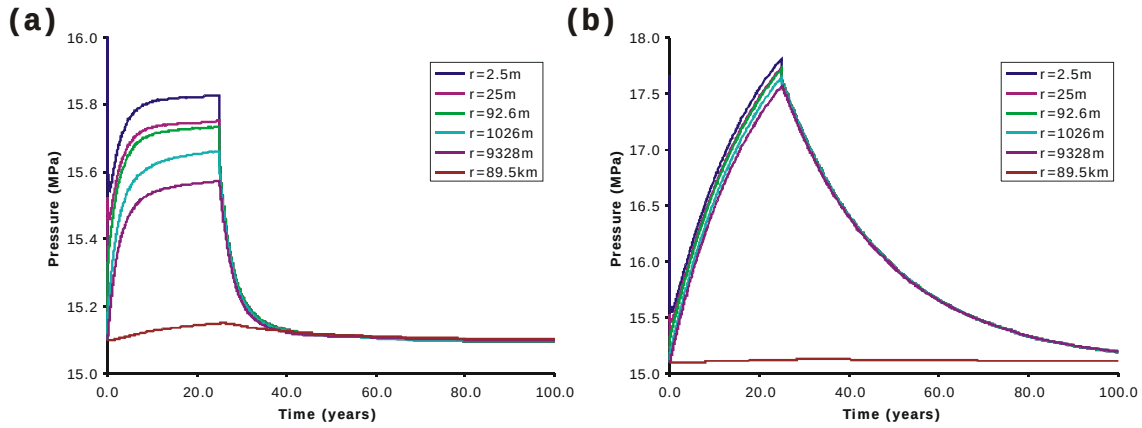

Figure 10 Pressures at selected points in a model with a cylindrical barrier at 10 km from the injection point. (a) 1m thick barrier with a permeability of 10^{-17} m^2. (b) 1m thick barrier with a permeability of 10^{-18} m^2.

Flow barrier at 1 km

In the previous simulations the flow barrier was located beyond the farthest spread of the CO_2 plume, which attained a radius of between 3 and 4 km. In consequence, there was no interaction of the CO_2 plume with the barrier, and pressure evolution largely reflected single-phase flow, as water was displaced by the laterally spreading plume. In this simulation a much smaller compartment of 1 km radius was considered. Here the CO_2 plume reached the barrier after about 4 to 5 years of injection with subsequent pressure evolution depending on the capillary pressure and relative permeability of the barrier material as well as its absolute permeability (Fig. 11a).

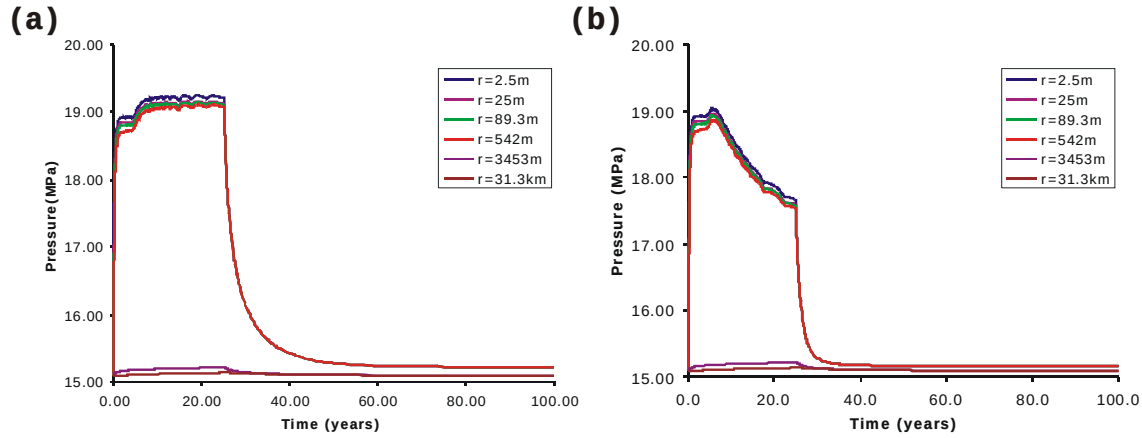

Figure 11 Pressures at selected points in a model with a cylindrical barrier at 1 km from the injection point. (a) The barrier is 1m thick with a permeability of 10^{-17} m^2 and P_0 = 2 MPa (see Equation 4). (b) The barrier is 1m thick with a permeability of 10^{-17} m^2 and P_0 = 100 kPa.

Due to the very small size of the injection compartment (3.14 km^2), pressures in this model were much higher than in previous models, rising rapidly to reach an initial steady-state of around 18.9 MPa within less than two years. However, after about five years, as the CO_2 plume reached the barrier, pressures increased again to reach a new steady-state level, some 0.3 MPa higher than before. This level was maintained, with some minor perturbations likely related to grid discretisation, until the injection of CO_2 was stopped. Subsequently, pressure decayed quite rapidly at first, but with a small residual elevated pressure at 100 years decaying very slowly.

A variation simulation, reducing the P_0 parameter for the barrier material (related to its capillary entry pressure) from the original 2 MPa to 100 kPa, shows markedly different results (Fig. 11b). Initially, the pressure evolved in just the same way as before, but once the CO_2 plume reached the barrier a short rise in pressure gave way to a protracted, steady decline. This contrasts markedly with the modelled behaviour of the higher P_0 barrier (Fig. 11a), and is mainly due to the fact that relative permeability changes highly non-linearly with saturation. With a lower P_0 value, CO_2 saturations are able to rise higher, giving very much higher relative permeabilities which allow CO_2 to pass through the barrier much more easily. It is also notable that pressures quickly fell below the early steady-state pressure of ~18.9MPa, which corresponded to water flow through the barrier. This is presumably largely attributable to a lower resistance to flow for CO_2 due to its much lower viscosity. By the end of the injection period, the pressure in the compartment had dropped by about 1.4 MPa. Cessation of injection led to a rapid pressure decline throughout the compartment, leading to a relatively small pressure residual at 100 years decaying very slowly.

The relative permeability behaviour of low permeability rocks, such as would constitute the modelled flow barriers, is not well understood, and it is likely that real effects would differ from the simple situations described here. These simulations are designed to explore potential conceptual processes with the aim of illustrating the types of effect that may be encountered in real storage cases.

Caprock sealing effects

The initial simulations incorporating flow barriers were all run with very low caprock and underburden permeabilities (10^{-22} m^2) to ensure that these layers had a minimal influence on pressure evolution. In order to test for these potential effects, the earlier simulation with a barrier at 35 km and a permeability of 10^{-18} m^2 , was re-run with just the caprock layer permeability increased by three orders of magnitude to 10^{-19} m^2 (Fig. 12a), the underburden remaining unchanged. Compared to the model with the lower permeability bounding layers (Fig. 9b), pressures reached within the compartment were somewhat reduced during the injection phase. More significantly, pressure decline after injection was noticeably more rapid, with the residual pressure excess at 100 years almost completely eliminated.

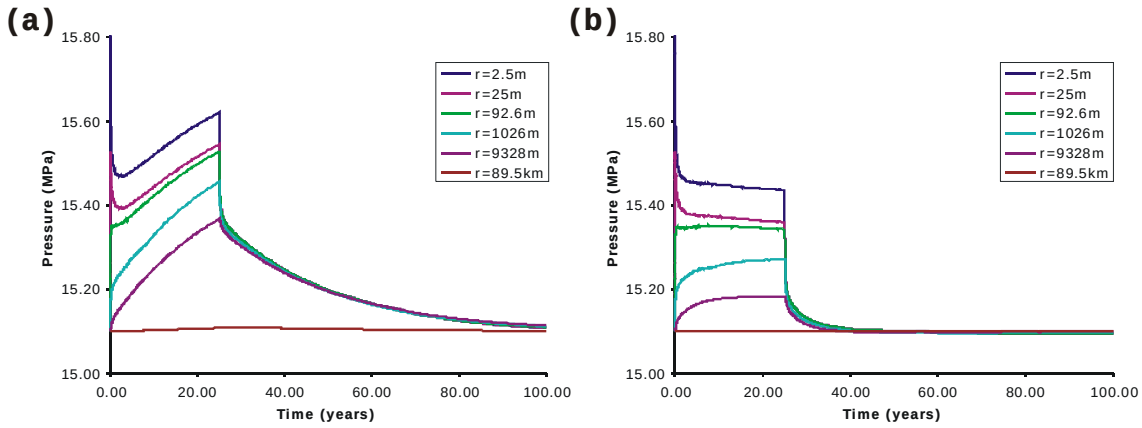

Figure 12 Pressures at selected points in a model with a cylindrical barrier at 35 km from the injection point, 1 m thick, with a permeability of 10^{-18} m^2. (a) The caprock layer has a permeability of 10^{-19} m^2. (b) Caprock layer has a permeability of 10^{-18} m^2.

Further increasing caprock permeability to 10^{-18} m^2 (Fig. 12b) eliminated all medium-term pressure build-up in the near-field during injection, such that after the initial transient, pressure close to the injection point declined slightly with time up to the end of injection at 25 years. Subsequently pressures decayed rapidly with no residual pressure elevation after about 50 years. At larger distances from the injection point (r = 89.5 km), the higher permeability of the caprock allows the pressure to dissipate completely, with little or no discernible response.

Similar effects are seen in the pressure history for a simulation with a barrier at 10 km from the injection point and permeability of 10^{-18} m^2 and a caprock permeability of 10^{-19} m^2 (Fig. 13). Once again the peak pressures are reduced compared with the initial 10 km barrier simulation (Fig. 10b) and the post-injection pressures decay rapidly such that there is no significant residual at 100 years.

It is clear that, particularly in reservoirs with barriers to lateral flow whose permeability is of the same order as the permeability of the bounding stratigraphical units, the flow properties of these units can be significant. In these cases, expulsion of water (via single-phase flow) through the reservoir sealing units can play an important part in reducing pressure increase.

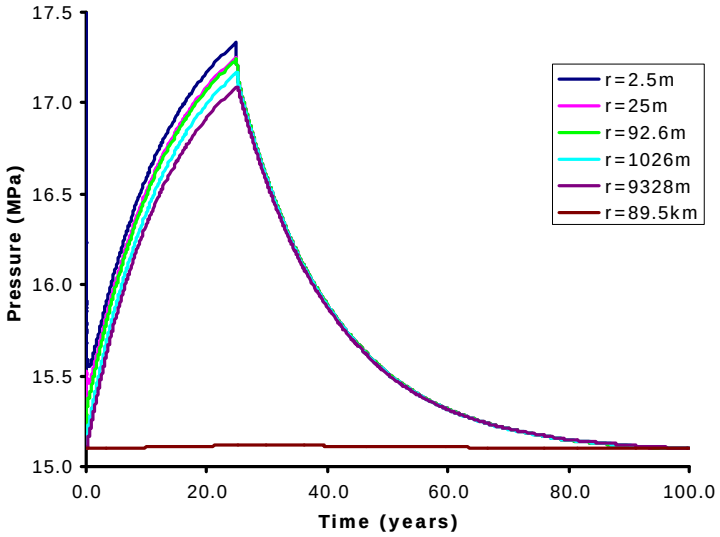

Figure 13 Pressures at selected points in a model with a cylindrical barrier at 10 km from the injection point, 1 m thick, with a permeability of 10^{-18} m^2 and the caprock layer has a permeability of 10^{-19} m^2.

APPLICATION OF THE MODELLING TO A REAL STORAGE CASE

In order to test the applicability and implications of the generic modelling approach, it is instructive to apply the methodology to a real aquifer storage site. An excellent current example is at Sleipner, in the North Sea, where StatoilHydro and partners are injecting CO_2 into a very large, high permeability sandstone aquifer.

Sleipner is the world's first industrial scale CO_2 injection project designed specifically as a greenhouse gas mitigation measure (Baklid *et al.* 1996). CO_2 separated from produced natural gas is being injected into the Utsira Sand, a major saline aquifer some 26000 km^2 in area (Fig. 14a). Injection started in 1996 and is planned to continue for about twenty years, at a rate of nearly 1 Mt per year. CO_2 is being injected into the Utsira reservoir via a deviated (near-horizontal) well, through a 38 m-long well perforation interval 1010-1013 m below sea level (bsl), and about 2.3 km from the platform. The injection point is close to the base of the Utsira Sand, about 200 m below the reservoir top, and beneath a gentle domal closure (Fig. 14b). By early 2008 more than ten million tonnes of CO_2 had been injected.

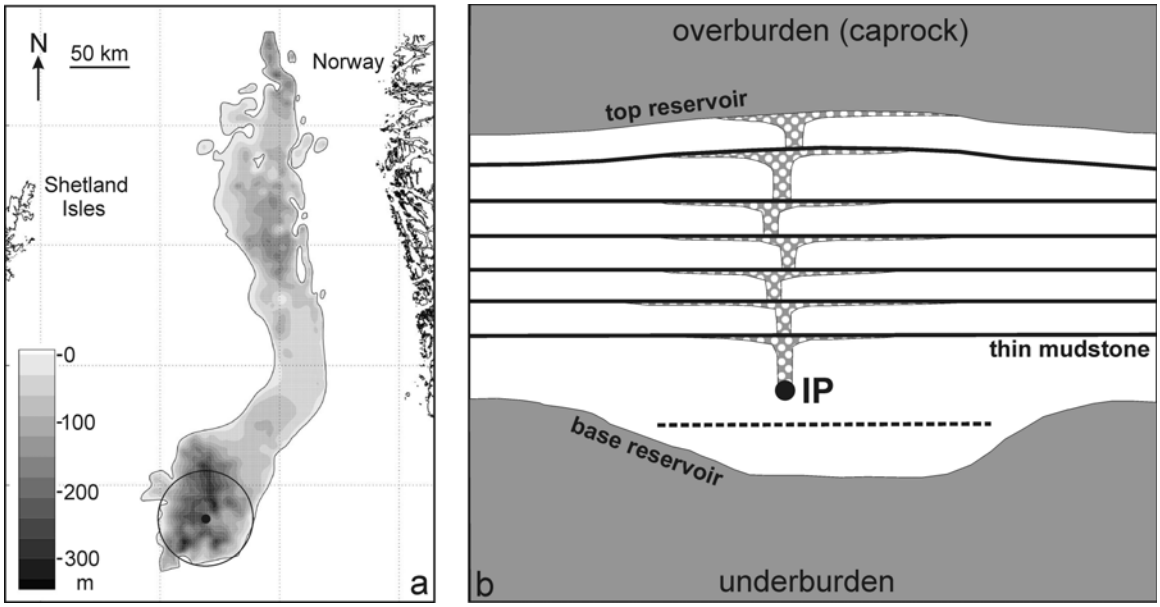

Figure 14 a) Thickness map of the Utsira Sand and the Sleipner injection point (black spot). Circle denotes 40 km radius around the injection point. b) Schematic diagram of the Utsira reservoir and the Sleipner CO_2 plume (spotted ornament). IP = injection point.

3D time-lapse seismic monitoring data (e.g. Arts *et al.* 2004; Chadwick *et al.* 2004b) image the CO_2 plume as a prominent multi-tier feature, comprising a number of bright sub-horizontal reflections, growing with time (Figure 15a). The reflections are interpreted as arising from a number of discrete layers of high saturation CO_2, each up to a few metres thick. The layers have mostly accumulated beneath thin intra-reservoir mudstones (seen on well logs, Figure 15b), with the uppermost layer being trapped beneath the reservoir caprock. Laboratory testing of caprock core samples (Harrington *et al.* in press) indicates that it will form a satisfactory capillary seal to free CO_2.

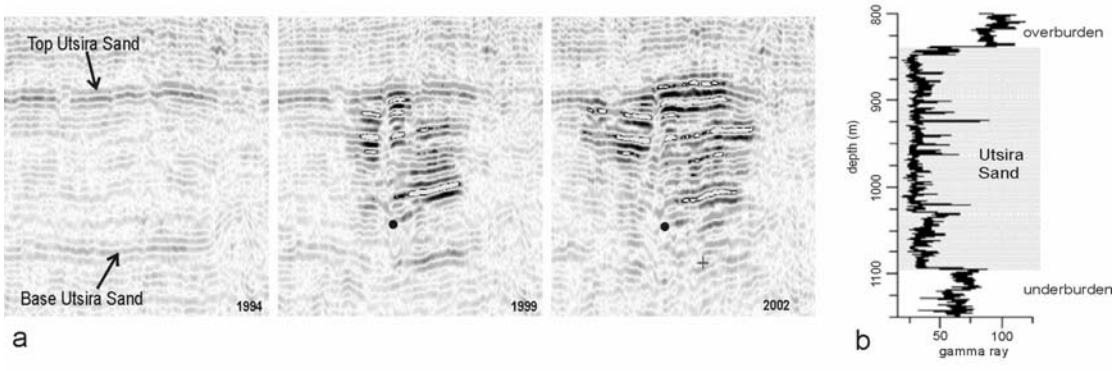

Figure 15 a) Time-lapse seismic lines at Sleipner showing growth of the CO_2 plume from 1994 (prior to injection) to 2002 b) γ-ray log through the Utsira Sand showing low γ-ray readings in the sand reservoir and γ-ray peaks corresponding to thin intra-reservoir mudstones.

A simplified model of the Sleipner injection experiment was constructed to test the injectivity of the Utsira reservoir. The assumption of cylindrical symmetry was retained, with a reservoir formation 250 m thick with its top at 800 mbsl. The reservoir properties are based on geophysical log data and a limited amount of core. Permeability was set at 2 $x10^{-12}$ m^2 (2 Darcy), the porosity at 37% (Zweigel *et al*. 2004) and the temperature at the top of the formation assumed to be 35 ºC (cf. Nooner *et al.* 2007). The reservoir formation was capped and underlain by 50 m thick layers with a permeability of $3x10^{-19}$ m^2, consistent with measured values for the caprock (Harrington *et al.* in press). The full set of parameter values used in the TOUGH2 models is given in Table 4.

Table 4 *Parameter values used in TOUGH2 models of the Sleipner case study.*

	Reservoir sand	**Caprock/ underburden**	**Barrier**
Permeability	$2x10^{-12}$ m^2	$3x10^{-19}$ m^2	$3x10^{-19}$ m^2
Porosity	0.37	0.32	0.37
Rel. perm. model			
λ	0.4	0.4	0.4
S_{lr}	0.2	0.2	0.2
S_{gr}	0.05	0.05	0.05
P_{cap} model			
λ	0.4	0.4	0.4
S_{lr}	0.19	0.19	0.19
P_0	4 kPa	1 MPa	400 kPa
P_{max}	6 MPa	6 MPa	6 MPa

CO_2 injection was simulated for 20 years at a constant rate of 28.16 $kg.s^{-1}$ (0.89 $Mt.yr^{-1}$) at a depth of 1012 mbsl and with a reservoir temperature at the injection point of 41 ºC. In the model, injection was into a single mesh element of radius 5 m and a height of 2 m, whereas in the field CO_2 is injected along a 38 m perforated horizontal length of the well. The use of the cylindrically symmetric model precludes a more realistic representation of the wellbore, but the result is that pressures in the immediate vicinity of the injection point may be expected to differ significantly between the model and the field situation. Differences should however decline with distance from the injection point so that model results at both r = 2.5 m and 25 m were plotted.

Unbounded and bounded reservoir

An initial Sleipner model was run with no boundary to the horizontal extent of the reservoir. Aside from the initial transient, pressures calculated from this ‘infinite aquifer’ model show essentially unchanging values over the injection period (Figure 16).

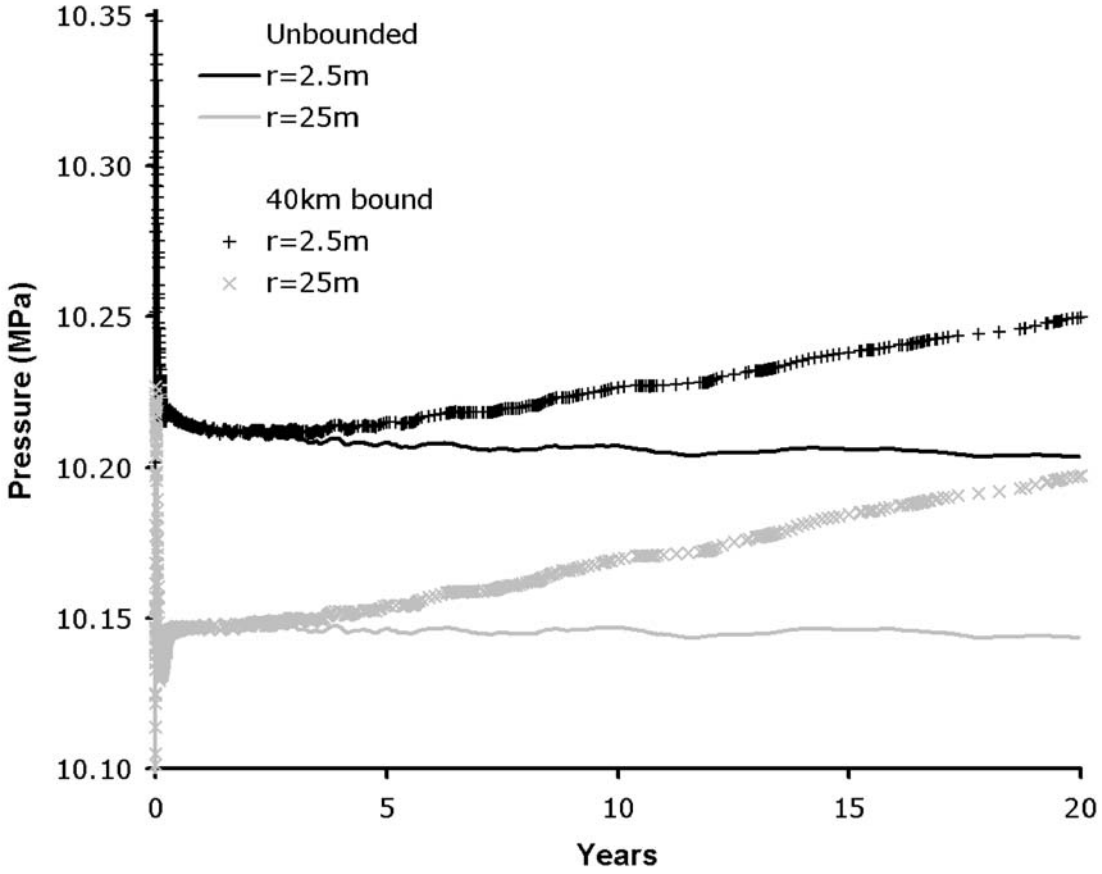

Figure 16 Calculated pressures in the vicinity of the injection point for an unbounded Utsira model and for a model with a barrier (boundary) 40 km from the injection point.

A second Sleipner model was run in which a vertical flow barrier, 1 m thick with an assigned permeability of $3x10^{-19}$ m^2 (same as the permeability of the caprock and the underburden), was placed through the reservoir at a distance of 40 km from the injection point. This could simulate the stratigraphical limit of a notional circular aquifer of similar dimensions to the southern part of the Utsira Sand (Fig. 14a). Results from the bounded model (Fig. 16) show that the flow barrier starts to noticeably affect pressures close to the injection point after about two years or so, but the pressure increase is quite small, about 0.05 MPa after 20 years.

Stratigraphical flow barriers

The Utsira Sand reservoir at Sleipner is not homogeneous sand, but, as illustrated above contains a number of thin mudstones with CO_2 ponded beneath. Logs from numerous well penetrations in the Utsira Sand indicate that the mudstones are laterally impersistent, individual mudstone units not generally being correlatable from well to well (wells are typically a few kilometres apart). These relatively impermeable mudstones may significantly affect pressure build up during the injection process by limiting the effective thickness of reservoir formation available to flow. Interpretation of time-lapse seismic data indicates that the injection point lies around 30 – 40 m

below the deepest CO_2 accumulation and about 60 m above the local base reservoir (Arts *et al.* in press), suggesting that the lowest sand unit is, at most, around 100 m thick. In fact its effective thickness is likely to be considerably less than this. The injection point was located above a localised depression in the base reservoir surface (Fig. 14b; Zweigel *et al*. 2004); elsewhere in the local area, the reservoir base commonly rises to about the elevation of the injection point, constraining the thickness of the lowest sand unit to 40 m or less. In addition there may well be one or more mudstone layers beneath the injection point, reducing the effective reservoir thickness still further. To provide an approximate minimum limiting bound on the effect of the mudstone layers, a third model was created in which the reservoir thickness was reduced to 50 m, to represent the sand unit into which the CO_2 is being injected. This model retains the outer flow barrier at 40 km as used in the previous model. Modelled pressure increase, at 0.09 MPa over twenty years (Figure 17), is higher than with the full thickness aquifer, but still quite small. Given that reducing aquifer thickness to 50 m represents an extreme parameter shift compared to the likely effect of the observed, laterally impersistent, mudstone layers (which are only around 1 m thick), it is evident that stratigraphical flow barriers in the Utsira Sand are unlikely to reduce injectivity significantly.

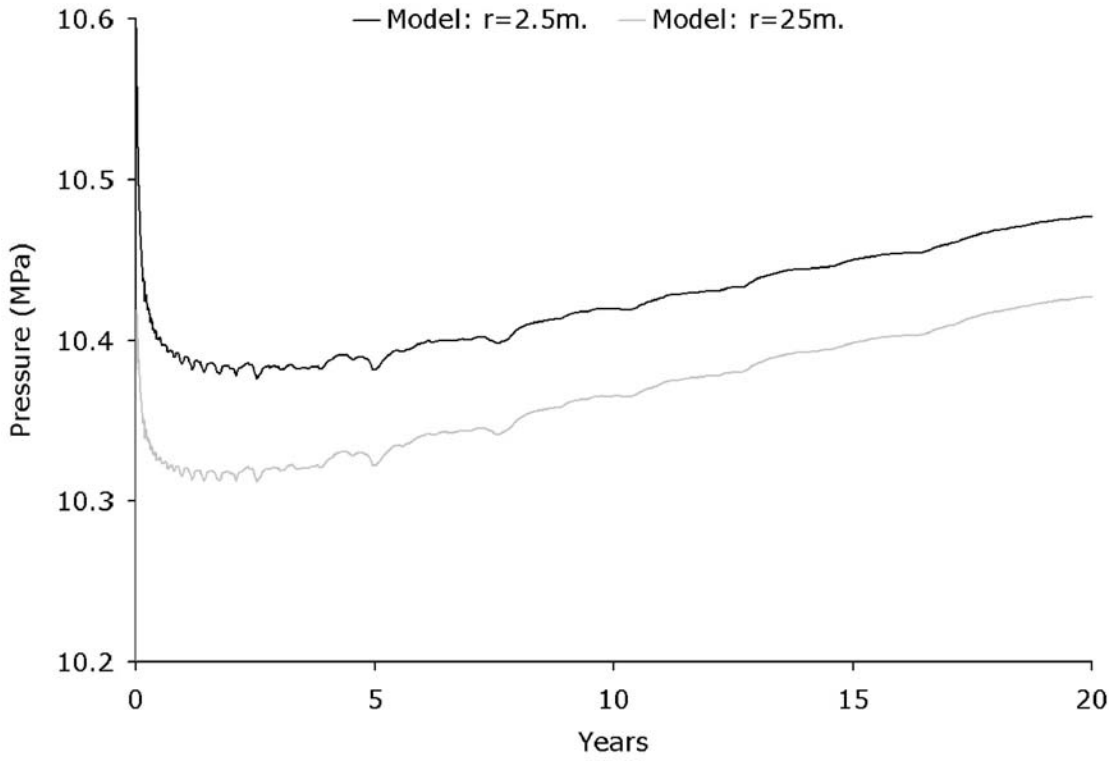

Figure 17 Modelled pressures for a 50 m thick reservoir bounded at 40 km from the injection point.

Structural flow barriers

It is instructive to explore the possible effects of structural compartmentalisation (faulting) within the reservoir. Zweigel *et al.* (2004) have noted considerable topography at the base of the Utsira Sand due to sediment mobilization in the argillaceous underburden. This has led to widespread post-depositional differential compaction within the reservoir, with the likelihood of vertical shear and associated

small-scale faulting. This is supported by Chadwick *et al.* (2004c), who noted that the seismically reflective CO_2 actually illuminates hitherto unresolved detail of reservoir internal architecture, revealing signs of small steep faults, close to the limit of seismic detectability, within the CO_2 plume itself.

In a generally clean sandstone such as the Utsira Sand, small faults with displacements considerably less than a few metres would likely be manifest as granulation seams or cataclastic deformation bands (Fowles & Burley 1994). From laboratory measurements, granulation seams in clean sandstone are quoted as having permeability reduction factors typically of around 10^{-4} compared to unfaulted country-rock, though occasionally down to 10^{-6} (e.g. Antonellini & Aydin 1994; Fisher & Knipe 2001; Lothe *et al.* 2002). According to Fossen *et al*. (2007), in a relatively shallow and poorly-consolidated formation such as the Utsira Sand, the most likely deformation features would be disaggregation bands with a permeability reduction factor of 10^{-1} or less. However, the presence of mica, chlorite and clays may allow the development of phyllosilicate bands, with potentially much higher permeability reduction factors (10^{-1} to 10^{-5}). For the Utsira Sand this would imply fault permeabilities generally around ~ 2×10^{-17} m^2 or higher.

A fourth model was created with a flow barrier 1m thick, 10 km from the injection point. An extremely low permeability of 3×10^{-19} m^2 was assumed. Such a flow barrier would be the equivalent of a cumulative thickness of >600 m of granulation seams (of permeability 2×10^{-16} m^2), which are interconnected and cannot be by-passed by the flow. Such an extreme flow barrier effect is difficult to visualise within 10 km or so of the injection point, but swarms of granulation seams in very close proximity to the injection point would have a proportionately greater effect and could significantly enhance local pressure elevation.

Modelled pressures (Figure 18) increase by about 0.8 MPa over twenty years. Bearing in mind the extremely conservative (pessimistic) properties of the modelled structural barrier, this is still a quite modest pressure increase.

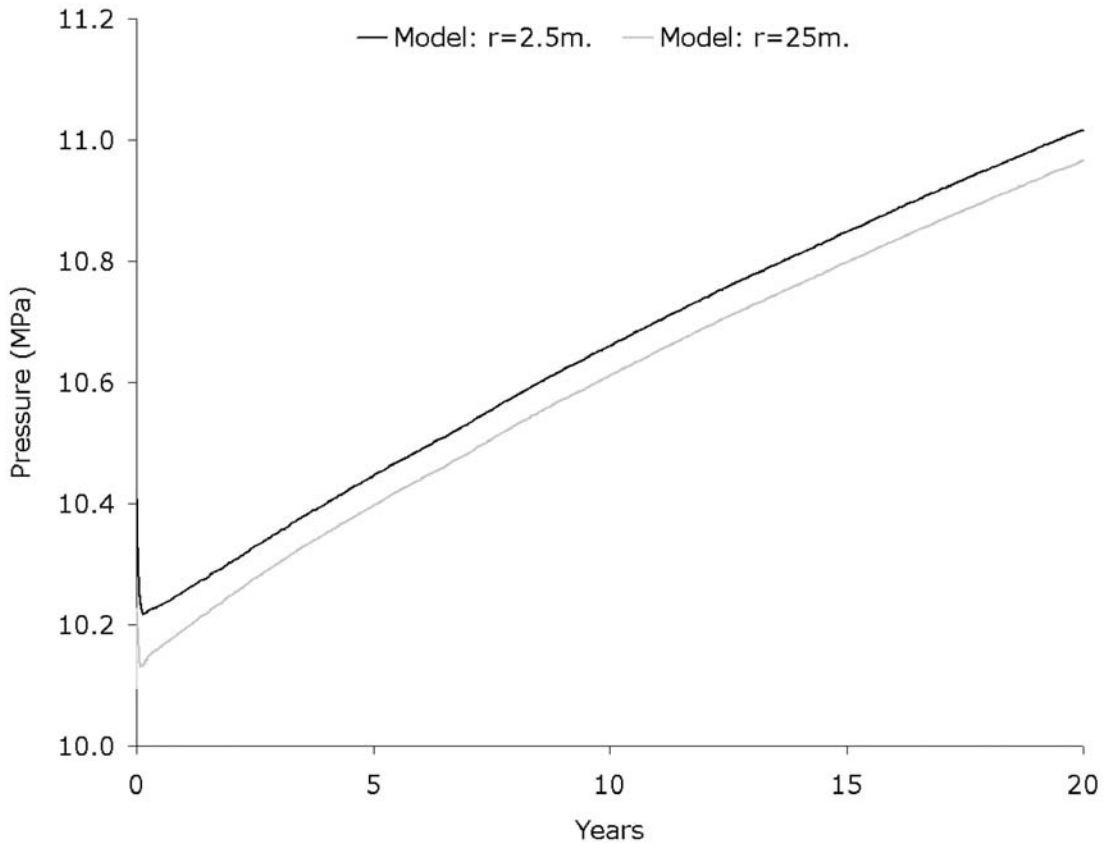

Figure 18 Modelled pressures for a reservoir with a flow barrier at 10 km from the injection point.

Overall, the Sleipner modelling indicates that any reservoir pressure changes likely to occur with the current CO_2 injection operation will be very small, around 0.1 MPa or less. Even the model incorporating improbably extreme structural compartmentalisation predicts modest pressure rises of less than 1 MPa.

Observed pressures

Although no reservoir pressure readings have been taken at Sleipner, wellhead pressures have been measured since the start of injection in 1996 (Figure 19).

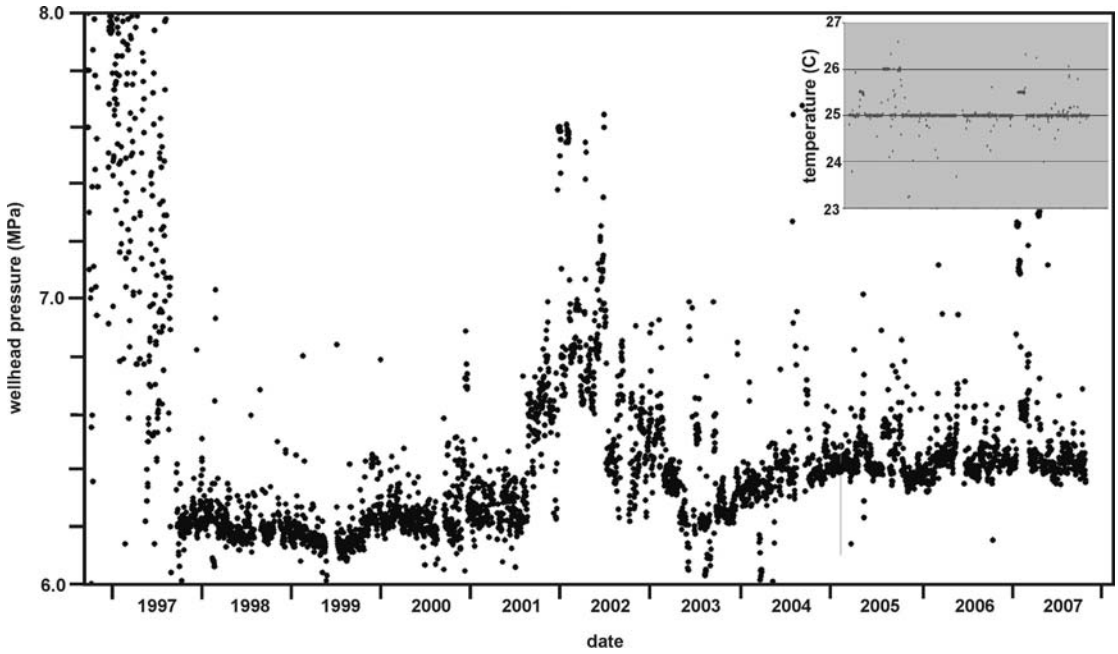

Figure 19 Wellhead pressures and temperatures (inset), measured at Sleipner, 1996 to 2007.

Two prominent features in the measured data are irregularly high pressures for the first few months and a prominent high pressure excursion from late 2001 to early 2003. These were caused by specific technical problems related to the injection infrastructure: the former due to sand blocking the perforation screens, an issue that was subsequently remediated, and the latter due to problems with the wellhead thermostatic temperature control (see below). Setting aside these anomalous readings, the wellhead data indicate early wellhead pressures of around 6.2 MPa (1997 to 2001) with rather higher pressures of around 6.4 MPa from about 2005 onwards.

Neglecting frictional effects associated with fluid transport down the well, downhole pressure at the injection point (approximating to near-wellbore formation pressure) is a function of the wellhead pressure and the weight of the CO_2 column in the wellbore:

$$P_{IP} = P_{WH} + g\int_0^Z \rho(z)dz$$

Where:
P_{IP} = downhole pressure at the injection point (depth Z)
P_{WH} = wellhead pressure (measured)
g = acceleration due to gravity
$\rho(z)$ = density of the injected CO_2 in the wellbore at depth z

Downhole pressure therefore depends on the density of the CO_2 column in the wellbore, which varies with temperature. Early in the injection history, CO_2 temperature at the wellhead was around 23 °C (Korbøl & Kaddour 1994), but from early 2005, measurements show accurate thermostatic control at 25 °C (Figure 19).

Downhole temperature measurements are not available, but calculations assuming adiabatic compression indicate that the CO_2 would be heated by about 32 °C as it moves down the wellbore to the injection point (Ola Eiken, Statoil, personal communication).

Looking first at the most recent pressure measurements (Figure 19), it is clear that from early 2005 onwards (years 8 to 10), there has been negligible systematic increase in wellhead pressure. Given that wellhead temperatures have been tightly controlled in this time period, it follows that downhole (and by implication reservoir) pressures have not increased significantly either.

To assess the longer-term observed wellhead pressure increase from 6.2 to 6.4 MPa, it is instructive to examine the effect of temperature changes on the CO_2 column in the wellbore. Assuming that the measured wellhead temperature increase, from 23 °C to 25 °C, is propagated down the temperature profile in the wellbore, CO_2 properties can be calculated using an equation-of-state. Densities calculated for a wellbore column comprising 98% CO_2 and 2% CH_4 (approximating the average injectant composition at Sleipner) indicate that a 2 °C increase in wellhead temperature would reduce average density in the CO_2 column by about 9 kgm^{-3}, thereby reducing the pressure due to the column by about 0.1 MPa. Thus, to maintain pressure at the injection point, wellhead pressures would have to be increased by the same amount. This can explain about half of the observed change in wellhead pressure, possibly more, acknowledging parameter uncertainty.

In addition to wellhead temperature changes, a longer-term effect concerns heat loss from the wellbore to the surrounding (cooler) rock formations. Heat loss would have been greatest at the start of injection, with a wellbore temperature profile rather cooler than the adiabatic. Since then, as the wellbore rock walls have gradually warmed, temperatures within the wellbore will also have increased, to progressively approach adiabatic. This would have the effect of decreasing column densities with time, reducing the pressure due to the wellbore column and increasing the wellhead pressure necessary to maintain downhole pressure. This effect would augment the effects of wellhead temperature change described above.

To conclude, it is likely that the wellhead pressure measurements at Sleipner are consistent with negligible pressure increase in the reservoir. In recent times, with wellhead temperatures closely controlled, wellhead pressures have remained roughly constant. The measured small increase in wellhead pressure in the longer term is explicable in terms of temperature changes of the CO_2 column in the wellbore. Very little, if any, increase in downhole pressure can be inferred from the wellhead measurents. This is consistent with the results of the flow simulations, indicating that the Utsira Sand is behaving as a very large aquifer with negligible internal flow barriers.

DISCUSSION

A likely key requirement of most large-scale aquifer storage projects is that the injection process does not raise fluid pressures to a level where damage to the storage system may occur (for example through tensile or shear failure of the reservoir or

caprock). In the central North Sea, at shallow to moderate depths (<3000 m), formation fracture pressures are around 85% of the lithostatic pressure (Moss *et al.* 2003). More typically, from worldwide data, fracture pressure is empirically stated to be about 80% of the lithostatic pressure. For storage situations in initially hydrostatically pressured aquifers at relatively shallow depth, the lithostatic (overburden) pressure will be around twice the value of the initial formation fluid pressure. Consequently, formation fracture pressure would be expected to be around 60% above hydrostatic.

The simulations show that for reservoirs without flow barriers, low injection rates into simple, thick, high permeability aquifers, pressure will likely not be an issue. Injection rates up to 10 $Mt.yr^{-1}$ typically produce pressure increases of <20% in reservoirs with permeabilities of > 1 Darcy (Fig. 5).

In the presence of flow barriers, the situation is more complex. Flow compartmentalisation, with permeability barriers to single-phase (water) flow, will significantly increase induced pressure effects even at relatively low injection rates (Fig. 10), with elevated pressures persisting for several decades after the cessation of injection. The situation would be further exacerbated for larger total storage amounts (greater than the 25 Mt considered in the simulations) and for low to medium permeability aquifers (Figs. 3 and 4).

A number of factors will have a generally favourable effect in terms of the induced pressure rise and its consequences. For example, injection via multiple wells will reduce the near-field effects of high total injection rates. In any case, pressure effects farther afield in the reservoir will be significantly less than close to the injection well(s). Taking the simulations as a whole, pressure increase at a distance of 9 km or so from the injection point is typically less than 60% of the pressure increase close to the injection point (except for the cases with very low permeability barriers). In many cases, reactivation-prone faults will lie a considerable distance from the injection point (e.g. Rogers *et al.* in press), in those areas where induced pressure increases are smaller. A key requirement for a storage reservoir would be that its caprock forms a capillary seal to free CO_2 (established during the site characterisation and selection process). But even where this is the case, pressure rise can be ameliorated by the process of (single-phase) water flow through the reservoir caprock and underburden.

More complex pressure evolutions are possible when free CO_2 itself interacts with the permeability barriers and two-phase flow effects become significant. Low permeability water-wet barriers can lead to significant additional pressure elevation. Conversely semi-permeable barriers can, in time, allow enhanced flow of low viscosity CO_2, reducing pressures around the plume.

Conceptually very simple flow barriers have been incorporated into the models at this stage. These comprised 1 m thick features, with permeabilities of 10^{-18} m^2 to 10^{-17} m^2, and laterally continuous (in terms of being wholly circumferential to the injection point). Regional studies of groundwater extraction in NW England indicate the presence of large-scale aquifer flow barriers, interpreted as corresponding to fault zones. These have properties equivalent to 1m thick barriers with permeabilities in the range 10^{-16} to 10^{-15} m^2 (Seymour *et al.* 2006). The barriers modelled herein therefore

are reasonably tight, with conservative (pessimistic) flow properties, in terms of their propensity to induce undesirable pressure effects.

Detailed flow modelling of fault zones is exceedingly difficult due to their very complex internal structure (e.g. Jones *et al.* 1998). Faults in a sandstone aquifer can vary from a more-or-less simple single slip surface to complex zones ranging in width from a few centimetres to several metres and typically comprising a central fault core of slip surfaces, gouges, lenses, breccias, cataclasites, clay smears and secondary mineralization, surrounded by dispersed damage zones of minor faults, factures, granulation seams, veins etc. Granulation seams, or cataclastic deformation bands (Fowles & Burley 1994), are particularly problematical. Though typically just a few millimetres thick and associated with very small displacements, they commonly occur in clusters or swarms, and can produce major features with significantly reduced permeability that may be all but invisible on seismic reflection data. Laboratory studies show permeability decreases from these types of feature ranging from 1 to more than 6 orders of magnitude. Clearly fault zones with many tens or even hundreds of such deformation bands will have significantly reduced bulk permeability. Upscaling such multiple, millimetre-scale, and perhaps laterally impersistent, features into an equivalent cell permeability for numerical simulation purposes is highly problematical (e.g Walsh *et al*. 1998; Berg & Øian 2007), and beyond the scope of this current paper. Away from the free CO_2 plume, we are mainly interested in single-phase (water) flow through much of the reservoir, so it may be that more empirical information from regional hydrogeological studies (e.g. Seymour *et al.* 2006) can provide key insights into the flow properties of typical basin-scale fault zones.

In this paper relatively little account has been taken of stratigraphical heterogeneity. This will likely be a significant feature of many future storage reservoirs and limited connectivity between stratigraphically-bounded storage compartments will significantly increase injection pressures. The issue of how detailed reservoir properties can be upscaled effectively into a simulation grid (e.g. Chen *et al.* 2003), is a subject of considerable current research, and again, is beyond the scope of this current paper.

More complex issues around reservoir engineering, such as multiple injection wells, and alternating CO_2-water injection strategies have not been discussed here.

CONCLUSIONS

A generic simulation approach has been taken to examine the main factors influencing reservoir-scale fluid flow whilst injecting supercritical CO_2 into high permeability saline aquifers. For this preliminary study, modelling has deliberately been kept simple, with a stepwise variation of parameters, to try to isolate and evaluate the principal factors controlling reservoir pressure evolution. It is clear that this involves dominantly hydrogeological (single-phase flow) processes throughout much of the storage reservoir and surrounding adjacent strata, with additional two-phase flow effects around the CO_2 plume itself.

Initial simulations looked at flow processes in an aquifer without explicit barriers to flow. Subsequent modelling explored the effects of incorporating discrete flow barriers at varying distances from the injection point. Key effects noted have been an initial pressure transient around the injection point, general pressure increase in the reservoir during the injection phase, and typically rapid pressure decline on cessation of injection.

Aquifers without flow barriers

After an initial pressure transient, avoidable by suitably ramping the initial injection flux, peak (long-term) injection pressure is a function of the injection rate and duration, and an inverse function of the reservoir permeability. Porosity influences the timescale of the initial pressure transient, but has relatively little independent effect upon the longer term pressure buildup.

For CO_2 injection into a simple, thick (>200m), high permeability (> 1 Darcy) aquifer, pressure rise will probably not be an issue, injection rates up to 10 $Mt.yr^{-1}$ typically producing near-field pressure elevations of <20% in reservoirs with permeabilities of > 1 Darcy. Pressure rise can be further ameliorated by the process of single-phase flow of water through the reservoir caprock and underburden, even though the former is likely to form an effective capillary seal to free CO_2.

Aquifers with flow barriers

Simulations of the more generally applicable case of injection into an aquifer with permeability barriers show significantly greater potential for induced pressure increase. It is clear that for higher injection rates (>10 $Mt.yr^{-1}$), into structurally or stratigraphically complex reservoirs, very careful site characterisation involving downhole pressure testing and numerical simulations will likely be required prior to the full operational phase. A potentially important process in constraining pressure rise in compartmentalised reservoirs is water flow from the aquifer via its stratigraphical seals. Single-phase flow into and through the caprock is likely to occur. Perhaps more importantly, the presence of a relatively high permeability underburden would be a desirable factor in the context of initial site selection and characterisation.

The ongoing CO_2 injection operation at Sleipner provides a valuable case-study with which to test these concepts of reservoir fluid flow. Measured wellhead pressures show a small non-systematic increase since the start of injection. This can be ascribed largely to temperature changes within the wellbore fluid column, with minimal inferred pressure increase in the reservoir. The Utsira Sand therefore is currently behaving as a large aquifer with no significant barriers to fluid flow.

ACKNOWLEDGEMENTS

We acknowledge valuable critical input from Peter Zweigel (StatoilHydro). This paper is published with permission of the Executive Director, BGS (NERC).

REFERENCES

Antonellini, M.A. & Aydin, A. 1994. Effect of faulting on fluid flow in porous sandstones: petrophysical properties. *American Association of Petroleum Geologists Bulletin*, 78, 355-377.

Arts, R., Eiken, O., Chadwick, R.A., Zweigel, P., Van Der Meer, L. & Kirby, G.A. 2004. Seismic monitoring at the Sleipner underground CO_2 storage site (North Sea). In: Baines, S., Gale, J. & Worden, R.J. (eds) *Geological Storage for CO_2 Emissions Reduction*. Special Publication of the Geological Society, London, 233, 181 - 191.

Arts, R.J., Chadwick, R.A., Eiken, O., Dortland, S., Trani, M. & Van Der Meer, L.G.H. (submitted). Seismic monitoring of the CO_2 storage at Sleipner sustained by synthetic modelling. In: Grobe, M., Pashin, J. & Dodge, R. (eds) *Carbon Dioxide Sequestration in Geological Media*. Special Publication of the American Association of Petroleum Geologists.

Baklid, A., Korbøl, R. & Owren, G. 1996. Sleipner Vest CO_2 disposal, CO_2 injection into a shallow underground aquifer. *SPE paper 36600, presented at 1996 SPE Annual Technical Conference and Exhibition*, Denver Colorado, USA, 6-9 October 1996.

Benson, S.L., Cook, P. J., Anderson, J., Bachu, S., Nimir, H. B., Basu, B., Bradshaw, J., Deguchi, G., Gale, J., von Goerne, G., Heidug, W., Holloway, S., Kamal, R., Keith, D., Lloyd, P., Rocha, P., Senior, W., Thomson, J., Torp, T., Wildenborg, A., Wilson, M., Zarlenga, F. & Zhou. D. 2005. *Chapter 5: Underground Geological Storage.* In: Metz, B., Davidson, O. Meyer L. &de Coninck H.C. (eds) *IPCC (Intergovernmental Panel on Climate Change): Special Report on Carbon Dioxide Capture and Storage.* Cambridge University Press, Cambridge, United Kingdom, 440 pp.

Berg, S.S. & Øian, E. 2007. Hierarchical approach for simulating fluid flow in normal fault zones. *Petroleum Geoscience*, 13, 22-35.

Chadwick, R.A., Zweigel, P., Gregersen, U., Kirby, G.A., Johannessen, P.N. & Holloway, S. 2004a. Characterisation of a CO_2 storage site: The Utsira Sand, Sleipner, northern North Sea. *Energy*, 29, 1371-1381. Elsevier Science Ltd, Oxford.

Chadwick, R.A., Arts, R., Eiken, O., Kirby, G.A., Lindeberg, E. & Zweigel, P. 2004b. 4D seismic imaging of an injected CO_2 bubble at the Sleipner Field, central North Sea. In: Davies, R.J, Cartwright, J.A, Stewart, S.A., Lappin, M. & Underhill, J.R. (eds.) *3-D Seismic Technology: Application to the Exploration of Sedimentary Basins.* Memoir of the Geological Society, London, 29, 305-314.

Chadwick, R.A., Holloway, S., Brook, M. & Kirby, G.A. 2004c. The case for underground CO_2 sequestration in northern Europe. In: Baines, S., Gale, J. & Worden, R.J. (eds) *Geological Storage for CO_2 emissions reduction.* Special Publication of the Geological Society, London, 233, 17 - 28.

Chadwick, R.A., Arts, R., Bernstone, C., May, F., Thibeau, S & Zweigel, P. 2008. *Best Practice for the Storage of CO_2 in Saline Aquifers*. (Keyworth, Nottingham:

British Geological Survey Occasional Publication No. 14.) ISBN: 978-0-85272-610-5. 277 pp.

Chen, Y., Durlofsky, L.J., Gerritsen, M. & Wen, X.H. 2003. A Coupled Local-Global Upscaling Approach for Simulating Flow in Highly Heterogeneous Formations. *Advances in Water Resources*, 26, 1041-1060.

Chilingar, G.V., Main, R. & Sinnokrot, A. 1963. Relationship between porosity, permeability and surface areas of sediments. *Journal of Sedimentary Geology*, 33/3, 759-765.

Corey, A.T., 1954. The interrelation between Gas and Oil Relative Permeabilities. *Producers Monthly*, November 1954, 38-41.

Czernichowski-Lauriol, I., Rochelle, C.A., Brosse, E., Springer,N., Bateman, K., Kervevan, C., Pearce, J.M., Sanjuan, B. & Serra, H. 2003. Reactivity of injected CO_2 with the Utsira Sand reservoir at Sleipner northern North Sea. In: Gale, J. & Kaya, Y. (eds) *Greenhouse Gas Control Technologies*, Pergamon, Amsterdam, 1617 - 1620.

Ennis-King, J. & Paterson, L. 2001. Reservoir Engineering Issues in the Geological Disposal of Carbon Dioxide. In: Williams, D., Durie, B., McMullan, P., Paulson, C., & Smith, A. (eds) *Proceedings of the 5th International Conference on Greenhouse Gas Control Technologies*. CSIRO, Collingwood, Australia, 290–295.

Fisher, Q.J. & Knipe, R.J. 2001. The permeability of faults within siliciclastic petroleum reservoirs of the North Sea and Norwegian Continental Shelf. *Marine & Petroleum Geology*, 18, 1063 – 1081.

Fossen, H., Schultz, R.A., Shipton, Z.K. & Mair, K. 2007. Deformation bands in sandstone: a review. *Journal of the Geological Society, London*, 164, 755-769.
Fowles, J. & Burley, S. 1994. Textural and permability characteristics of faulted, high porosity sandstones. *Marine and Petroleum Geology*, 11/5, 608 – 623.

Harrington, J.F., Noy, D.J., Horseman, S.T., Birchall, D.J. & Chadwick, R.A. (in press) Laboratory study of gas and water flow in the Nordland Shale, Sleipner, North Sea. In: Grobe, M., Pashin, J. & Dodge, R. (eds) *Carbon Dioxide Sequestration in Geological Media*. Special Publication of the American Association of Petroleum Geologists.

Holloway, S. 2001. Storage of Fossil Fuel-Derived Carbon Dioxide Beneath the Surface of the Earth. *Annual Reviews of Energy and the Environment*, 26,145-166.

Hovorka, S. 2005. Testing efficiency of CO_2 storage in the subsurface: Frio Brine pilot project. In: Rubin, E. S., Keith, D. W. & Gilboy, C. F. *Proceedings of the 7th International Conference on Greenhouse Gas Control Technologies, Volume 2. Contributed papers and panel discussion*, Elsevier, Oxford, 1361–1366.

IPCC 2007. Climate Change 2007: The Physical Science Basis, Summary for Policymakers. http://www.ipcc.ch/SPM2feb07.pdf

Johnson, J.W. & Nitau, J.J. 2003. Reactive transport modeling of geologic CO_2 sequestration at Sleipner. In: Gale, J. & Kaya, Y. (eds) *Greenhouse Gas Control Technologies*, Volume 1, 337 - 332, Pergamon, Amsterdam.

Jones, G., Fisher, Q.J. & Knipe, R.J. (eds). 1998. Faulting and fault sealing in hydrocarbon reservoirs. *Special Publication of the Geological Society of London*. 319 pp.

Kikuta, K., Hongo, S., Tanase, D. & Ohsumi, T. 2005. Field test of CO2 injection in Nagaoka, Japan. In: Rubin, E. S., Keith, D. W. & Gilboy, C. F. *Proceedings of the 7th International Conference on Greenhouse Gas Control Technologies, Volume 2. Contributed papers and panel discussion*, Elsevier, Oxford, 1367–1372.

Korbøl, R. & Kaddour, A. 1995. Sleipner Vest CO_2 disposal – injection of removed CO_2 into the Utsira Formation. In: Kondo, J., Inui, T. & Wasa, K. (eds). *Proceedings of the second International Conference on Carbon Dioxide Removal*, Kyoto 24-27 October 1994. Pergamon, 519-512.
Law, D. 1996. Injectivity studies. In: Hitchon, B. (ed.) *Aquifer Disposal of Carbon Dioxide: Hydrodynamic and Mineral Trapping — Proof of Concept*. Geoscience Publishing, Sherwood Park, Alberta, Canada, 59–92.

Lindeberg. E. & Wessel-Berg, D. 1997. Vertical convection in an aquifer column under a gas cap of CO_2. *Energy Conversion and Management,* 38, (Supplement): S229-34.

Lindeberg, E., Zweigel, P., Bergmo, P., Ghaderi, A. & Lothe, A. 2001. Prediction of CO_2 dispersal pattern improved by geology and reservoir simulation and verified by time lapse seismic. In: Williams. D., Durie, B., McMullan, P., Paulson, C. & Smith, A. (eds) *Proceedings of the 5th International Conference on Greenhouse Gas Control Technologies*. CSIRO, Collingwood, Australia, 372-377.

Lothe, A.E, Gabrielsen, R.H., Bjørnevoll Hagen, N. & Larsen, B.T. 2002. An experimental study of the texture of deformation bands: effects on the porosity and permeability of sandstones. *Petroleum Geoscienc*e, 8, 195-207.

Moss, B., Barson, D., Rakhit, K., Dennis, H. & Swarbrick, R. 2003. Formation pore pressures and formation waters. In: Evans, D., Graham, C., Armour, A. & Bathurst, P. (eds). *The Millenium Atlas: Petroleum Geology of the Central and Northern North Sea*. Geological Society of London. 389pp.

Nooner, S.L., Eiken, O., Hermanrud, C., Sasagawa, G.S., Stenvold, T. & Zumberge, M.A. 2007. Constraints on the *in situ* density of CO_2 within the Utsira formation from time-lapse seafloor gravity measurements. *International Journal of Greenhouse Gas Control*, 1, 198-214. Elsevier.

Obdam, A, van der Meer, L.G.H., May, F., Kervevan, C., Bech, N. & Wildenborg, A. 2003. Effective CO_2 storage capacity in aquifers, gas fields, oil fields and coal fields. In: Gale, J. & Kaya, Y. (eds.) *Greenhouse Gas Control Technologies*, Volume 1, 339-352, Pergamon, Amsterdam.

Pruess, K. 2005. ECO2N: A TOUGH2 Fluid Property Module for Mixtures of Water, NaCl, and CO_2. *Lawrence Berkeley National Laboratory Report LBNL-57952.*
Pruess, K., Oldenburg, C. & Moridis, G. 1999. TOUGH2 User Guide, version 2.0. *Lawrence Berkeley National Laboratory Report LBNL-43134*.

Pruess, K., García, J., Kovscek, A., Oldenburg, C., Rutqvist, J., Steefel, C. & Xu, T. 2002. Intercomparison of numerical simulation codes for geologic disposal of CO_2. *Lawrence Berkeley National Laboratory Report LBNL-51813*.
Price, M. 1996. *Introducing Groundwater (2nd Edition)*. Prentice Hall, 278 pp.

Riddiford, F.A., Tourqui, A., Bishop, C.D., Taylor, B. & Smith, M. 2003. A cleaner development: the In Salah Gas project, Algeria. In: Gale, J. & Kaya, Y. (eds) *Greenhouse Gas Control Technologies*, Volume 1, 595-600, Pergamon, Amsterdam.

Rogers, C., van Ruth, P. & Hillis, R. (in press). Fault Reactivation in the Port Campbell Embayment with respect to carbon dioxide sequestration, Otway Basin, Australia. In: Johnson, H., Dore, A., Gatliff, R., Ritchie, D., Holdsworth, R. & Lundin, E. (eds). The Nature and Origin of compression on Passive Margins. *Special Publication of the Geological Society of London*.

Seymour, K.J., Ingram, J.A. & Gebbett, S.J. 2006. Structural controls on groundwater flow in the Permo-Triassic sandstones of NW England. In: Barker, R.D & Tellam, J.H. (eds). *Fluid Flow and Solute Movement in Sandstones: The Onshore UK Permo-Triassic Red Bed Sequence*. Special Publication of the Geological Society, London, 263, 169 – 185.

Span, R. & Wagner, W., 1996. A New Equation of State for Carbon Dioxide Covering the Fluid Region from the Triple-Point Temperature to 100 K at Pressures up to 800 MPa, *Journal of Physical and Chemical Reference Data*, 25/ 6, 1509 – 1596.

Van Genuchten, M.Th., 1980. A Closed-form Equation for Predicting the Hydraulic Conductivity of Unsaturated Soils. *Soil Science Society of America Journal*, 44, 892-898.

Walsh, J.J, Watterson, J., Heat, A.E. & Childs, C. 1998. Representation and scaling of faults in fluid flow models, *Petroleum Geoscience*, 4, 241-252.

Wilson, M. & Monea, M. 2004. *IEA GHG Weyburn CO_2 Monitoring & Storage Operation Summary Report 2000 - 2004*. Petroleum Technology Research Centre, Regina.

WMO 2006. WMO Greenhouse Gas Bulletin, No. 2, 1st November 2006. http://www.wmo.int/pages/prog/arep/gaw/ghg/documents/ghg-bulletin-en-11-06.pdf

Zweigel, P., Arts, R., Lothe, A.E & Lindeberg, E.R.G. 2004. Reservoir geology of the Utsira Formation at the first industrial-scale underground CO2 storage site (Sleipner area, North Sea). In: Baines, S., Gale, J. & Worden, R.J. (eds) *Geological Storage for*

CO_2 emissions reduction. Special Publication of the Geological Society, London, 233, 165 - 180.